Experimental Evidence of Correlations Between Conditioning and Relaxation in Hysteretic Elastic Media

M. Scalerandi,[1,*] C. Mechri,[2,3] M. Bentahar,[2,4] A. Di Bella,[1] A.S. Gliozzi,[1] and M. Tortello[1]

[1] *DISAT, Condensed Matter Physics and Complex Systems Institute, Politecnico di Torino, Turin, Italy*
[2] *LAUM UMR CNRS 6613, Le Mans Université, Le Mans, France*
[3] *CTTM, 20 Rue Thalis de Milet, Le Mans, France*
[4] *ENSIM, Le Mans Université, Le Mans, France*

(Received 13 June 2019; revised manuscript received 28 July 2019; published 1 October 2019)

Consolidated granular materials and materials with damage at the microstructural level exhibit anomalous elastic behavior even when excited by low-amplitude elastic waves. Their response is given by a combination of slow- and fast-dynamics effects which, as their definition implies, act on very different time scales. In particular, conditioning (a transition to an elastic state dependent on the strain amplitude) and relaxation (full recovery of the elastic properties when the strain is removed) have been observed in different materials and under different dynamic excitations. An experimental parametric analysis of the phenomenon, aiming to establish correlations between the effects on different elastic physical properties (wave velocity and attenuation coefficient) and between the evolution of conditioning and relaxation is proposed here, with the goal of better characterizing slow dynamics and allowing one to go beyond the phenomenological description of elastic hysteresis currently available. At the same time, by studying different materials, we wish to highlight the possibility of using slow dynamics as an additional tool for materials characterization.

DOI: 10.1103/PhysRevApplied.12.044002

I. INTRODUCTION

Nonlinear elasticity in materials is often associated with a loss of linearity in the stress-strain relation, which still keeps an analytic form, when the excitation amplitude becomes high. This description, usually known as classical nonlinear elasticity [1], however, fails in describing the anomalous elastic behavior observed in mesoscopic nonlinear elastic materials [2,3]. Consolidated [4–7] and unconsolidated [8] granular media not only show nonlinear elastic behavior at low strains but also feature, in addition, hysteresis in the stress-strain dependence, which can thus no longer be described by an analytic function. Furthermore, features typical of anomalous elasticity are also present in the response to ultrasonic excitation of damaged materials, whether granular [9,10] or not (metals, composites, etc.) [11,12].

A typical characteristic of hysteretic elastic behavior is the presence of features at the microscale level which produce physical effects on very different time scales (fast and slow dynamics). Fast dynamics [13–19] is generally associated with "instantaneous" variations of the elastic modulus and damping parameter [20,21]. Slow dynamics [22–24] is associated with completely different physical processes and can be described as follows: when a strain of fixed amplitude is applied, the wave velocity (referred to as simply "velocity" hereafter) and damping in the material evolve slowly to a new equilibrium value different from that of the unperturbed state. The phenomenon is fully reversible and, once the strain is removed, the system relaxes back to its original equilibrium state, that is, with the initial values of the material properties. Thus, slow dynamics is typical of nonequilibrium phenomena and of the related transients from one equilibrium state to another. We refer to conditioning [13,25–27] when the material rearranges its state as a consequence of an applied strain, and to relaxation [24,28–31] when it recovers, after a conditioning process, its original properties once the strain is no longer applied. Both processes take place over a long time scale.

From the point of view of fast dynamics, hysteretic elastic materials show, both qualitatively and quantitatively, a similar response, although with some differences, for example in the power-law exponent describing nonlinear dependencies [32,33]. From the physical point of view, however, they are characterized by very different microstructural features (partially open clapping microcracks [34], closed microcracks with adhesion forces [35], sliding or frictional interfaces [36,37], etc.). Thus, it is not clear whether a single universal mechanism or, rather, a specific material-dependent one should be identified as the origin of nonlinearity and nonequilibrium behavior. Since

*marco.scalerandi@infm.polito.it

conditioning and relaxation are distinctive features of hysteresis, their description could be crucial for validating nonphenomenological models [13,25,37–41].

Great attention has also been devoted recently to the use of slow dynamics as a general tool for characterizing nonlinear properties of materials and their evolution due to degradation or damage progression [42,43]. This is mainly due to the advantage that, from the experimental point of view, a single impact or "event" is sufficient to induce slow dynamics and that monitoring of the related effects could be done by means of low-amplitude probe signals (in other words, nonlinear effects can be probed by means of linear measurements) [43]. Therefore, differently from what happens with other approaches, possible nonlinearities due to the experimental setup and the need for careful control of source amplitudes would no longer be an issue to deal with in order to quantify nonlinear elastic properties. A very promising application in this regard is the possibility of investigating slow-dynamics effects triggered by ambient noise, as has been shown, for example, in the case of the effects of seismic and environmental loading on civil engineering structures [44]. At the same time, it has also been evidenced (mostly by using the dynamic acousto-elasticity testing approach) that the presence of damage is responsible for an increase in slow-dynamics effects compared with those observed in intact samples, in buildings [31], loaded [45] and thermally damaged concrete [46]. A generic increase in slow dynamics when damage is present is of course extremely interesting from the point of view of damage detection. Nevertheless, quantification, reliable assessment, and discrimination of different damage types are generally hard to achieve because comparable and well-controlled starting experimental conditions would be required. Indeed, differences in the spatial strain distribution within a sample, slight variations in environmental conditions, differences in the resonance frequency of samples tested, etc. could generally induce quantitative differences in the slow-dynamics response of intact samples that may be of the same order of magnitude as those caused by the presence of damage. Therefore, in order to make the analysis simpler and more reliable, an approach aimed at identifying different functional behavior in the response of intact vs damaged samples is highly desirable, as has been done, for example, in another context, where distinct power-law behavior for materials with different forms of damage has been reported [33].

The goal of this paper is (i) to define measurable quantities to characterize and quantify the temporal evolution of damping and velocity (slow dynamics), (ii) to provide methods for measuring their dependence on strain, and (iii) to establish correlations between them. Several experimental results, obtained on different types of consolidated granular materials, are presented with the aim of selecting, from among the measured quantities, those that better allow identifying differences between intact and damaged samples, thus indicating the possibility of distinguishing between classes of materials with different behavior. An extensive experimental analysis of the behavior of the damping and velocity as a function of time during conditioning or relaxation (and also by varying the conditioning strain amplitude) is presented. The possible emergence of relationships and correlations between indicators related to the damping and modulus or to conditioning and relaxation is discussed from the point of view of analyzing and validating the completeness, suitability, and "universality" of the models proposed in the literature. Furthermore, it is shown that damaged samples exhibit slow-dynamics effects similar to those observed in intact ones, but with significant differences (mostly in terms of a different functional dependence of the velocity and damping as a function of time). This result represents a promising step from the point of view of developing fast and accurate nondestructive testing tools for characterizing elastic nonlinearity of damaged samples.

II. MATERIALS AND METHODS

A. Experimental setup

The experiments are conducted by using a waveform generator (Tektronix AFG 3022B) to produce ultrasonic signals defined as monochromatic waves of amplitude A_{inp} and frequency ν. After amplification through a linear amplifier (CIPRIAN Model US-TXP-3, 200 x), the signals are transmitted to an ultrasonic transducer (with a broadband response, up to a few hundreds of kHz) acting as an emitter. The transducer is glued to the sample using phenyl salicylate (salol). A second (identical) transducer is used to detect the response of the material under test and is connected to a digital oscilloscope (Lecroy 324A) for data acquisition. The experiments are performed using MATEST C370-02 transducers (with a diameter of 2.5 cm) with a center frequency at 55 kHz, specifically designed for concrete samples.

The signals are recorded in a short time window once stationary conditions are reached (standing waves). In order to excite longitudinal modes (both transducers are excited in compressional mode), the transducers are glued on the base of the sample. The linearity of the acquisition system, including the transducers and coupling media, is verified by measuring a linear metallic sample (copper) and also the response of the two transducers coupled to each other by means of salol and exciting them within the same frequency and amplitude range. In the experiments discussed here, the frequency is always chosen close to the fundamental compression resonance mode of the samples and A_{inp} ranges from 10 mV to 1.2 V (before amplification).

B. Samples

We test several samples, representative of classes of materials with different structures at the microscopic level: (i) with distributed heterogeneity on the macroscopic scale (due to the presence of large inclusions in concrete) or on the microscale (due to the grain structure in mortar and sandstone), and (ii) with localized heterogeneity due to damage-induced microcracks (damaged concrete).

The characteristics of the samples investigated are the following:

(a) The concrete sample (B06) is in the shape of a cylinder (4 cm diameter and 16 cm length) and is drilled from a casting prepared with 340 kg of cement (CEM II A-L 42.5 R), 957 kg of sand (0–5 mm), 846 kg of gravel (5–15 mm), and 200 kg of water [water:cement (w/c) ratio ≈ 0.59]. The age of the cylinder at the time of testing is more than 5 years, thus guaranteeing that the cement hydration process is completed.

(b) The Berea Sandstone sample is a thin cylinder with a diameter of 2.5 cm and 15 cm long. The size of the grains in this sample is of the order of tens of micrometers.

(c) The mortar sample (P18) is in the shape of a prism ($4 \times 4 \times 16$ cm^3) and is produced using Portland cement (CEM I 42.5N) with a w/c ratio of 0.35 by mass.

(d) The damaged mortar sample (TQ4) is produced with the same Portland cement as sample P18 and a w/c ratio of 0.3. It is in the shape of a prism with a size of $3 \times 3 \times 15$ cm^3.

(e) The damaged concrete sample (X4) is produced with proportions of 2 volumes of cement, 4 volumes of sand, and 6 volumes of gravel per volume of water (the average gravel size is 7 ± 2 mm and the size of the sand particles is predominantly around 2 mm). Sample X4 is damaged by a quasistatic three-point bending test performed at 75% of its rupture load.

C. Data acquisition and analysis

The measurements are performed by using monochromatic waves and monitoring the system response over time. Each experiment consists in the following procedure: (i) A monochromatic wave with the lowest possible excitation amplitude is continuously sent to the sample, in order to avoid generation of slow-dynamics effects but still being above the noise level. Several portions of the output signals are subsequently recorded by repeating, at different times, the same temporal acquisition window, in order to monitor preconditioning. Then, (ii) the input amplitude is amplified to a new level, and acquisition is repeated at successive times, as in (i), but now to monitor conditioning effects. Finally, (iii) the amplitude is set back to the initial low-amplitude level to monitor relaxation dynamics. No delay times occur within the three steps. The protocol is described in Fig. 1.

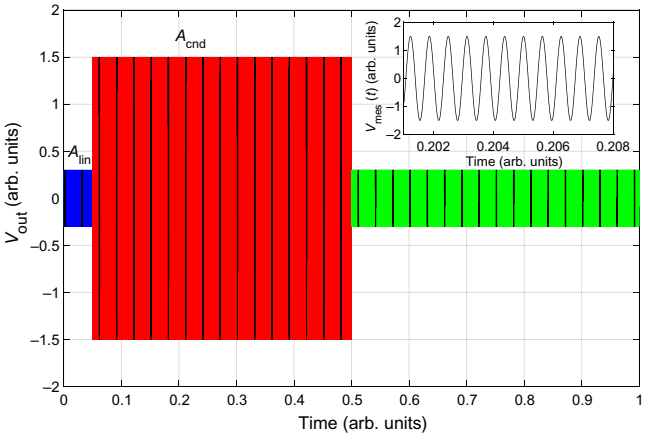

FIG. 1. Scheme of the experimental protocol. The graph shows the schematic output signal as a function of time for the three steps of the protocol: preconditioning (blue), conditioning (red), and relaxation (green). The vertical lines indicate the time windows of the signal that are acquired by the oscilloscope. Inset: example of a signal acquired during conditioning.

Measurements are performed by varying the amplification of the input signal during step (ii) in order to achieve a different level of conditioning. Then, full relaxation is allowed for several hours between protocols performed at increasing conditioning amplitudes.

For each time window (that is, at different times during the same measurement protocol), the recorded signal is analyzed following an approach which allows us to simultaneously extract the modulus and damping of the material. These two quantities can be obtained from the phase and amplitude of the recorded waveform when the distortions of the signals from a pure sinusoid are small, that is, for small nonlinearities [20]. The procedure adopted to derive the dependence of the velocity and damping on amplitude is reported in Appendix A1.

III. CONDITIONING AND RELAXATION

A. Experiments

Experiments are performed on the concrete sample B06, following the protocol discussed above. First, the sample is excited with a low-amplitude excitation A_{lin} (preconditioning). Then, the source amplitude is set to a conditioning-effective level A_{cnd} (conditioning). Finally, the source amplitude is set again to the initial value (relaxation). The scheme of the protocol is reported in Fig. 1. The signals are acquired using a fixed time window, $\Delta t = 5$ ms, at successive times. The detected signals are fitted to a cosine wave to extract the amplitude and phase as a function of time.

The variations of the normalized amplitude and phase with respect to the value at $t = 0$ s, i.e., the preconditioning equilibrium value, are shown in panels (a) and (b) of

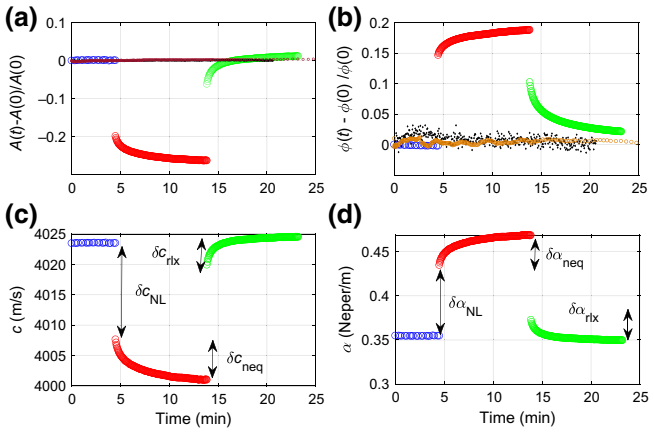

FIG. 2. Evolution of material properties as a function of time during a conditioning experiment. (a) and (b) show the evolution of the amplitude and phase of the harmonic signal detected by the receiver. (c) and (d) report the evolution of velocity and attenuation coefficient as a function of time. The sample is B06, the source frequency is set to 11.2 kHz, and the excitation amplitude during conditioning is $A_{\mathrm{cnd}} = 0.58$ V. The black and brown symbols in panels (a) and (b) show the signals acquired by directly coupling the two transducers and by measuring a linear sample (copper), respectively.

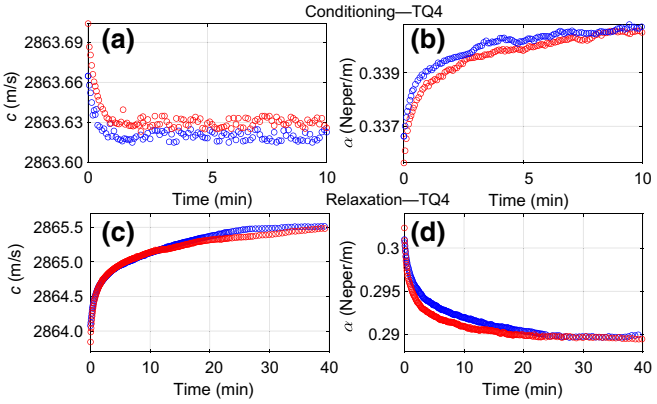

FIG. 3. Evolution of velocity and attenuation coefficient during conditioning and relaxation for sample TQ4. The same experiment is repeated on different days to prove reproducibility and robustness of the measurements. Here, the frequency is 19.82 kHz and the conditioning amplitude A_{cnd} is 1 V before amplification.

Fig 2. Both the transition to a new equilibrium state when the source amplitude is increased and the subsequent relaxation to the initial amplitude and phase values are evident. The same analysis is also performed on a linear metallic sample, consisting of copper (brown symbols), and by directly coupling the two transducers with salol without any sample in between (black symbols). As expected, both the normalized amplitude and the phase are constant as a function of time, that is, their variation with respect to the initial value is zero, thus demonstrating the linearity of the setup and of the acquisition procedure.

Then, from Eqs. (A4) and (A5) in Appendix A1, the velocity and damping can be derived, and their variations with respect to the preconditioning value are shown as a function of time in Fig. 2(c) and 2(d). As expected, we observe a softening and an increase in the attenuation during the conditioning phase, followed by a full relaxation. This indicates that the conditioning effect is fully reversible. The full evolution of c and α, characterized by introducing a few parameters indicated in Fig. 2(c) and 2(d), can be easily determined without making any assumption about the shape of the relaxation curve:

(a) Conditioning is characterized by an initial jump in the velocity, δc_{NL}, at $t = t_c$ due to nonlinear effects (see Fig. 2), where t_c is the time at which the conditioning amplitude is applied. For a given state of the material, this jump is dependent on the conditioning amplitude. Then, after the initial sudden variation in the velocity value, a slow-dynamics process takes place, until a new equilibrium state is achieved along with a further variation of velocity, δc_{neq}. Similar parameters are defined for α as well.

(b) Relaxation is characterized by a single parameter δc_{rlx} (and a similar one for α), which characterizes memory, that is, the residual effect of conditioning on the velocity and damping when the conditioning amplitude is turned off.

These parameters are discussed in more detail in Appendix A2.

The measurements performed during conditioning and relaxation have a high degree of repeatability, thus proving the robustness of the conclusions reported here. The measurements on sample TQ4 are repeated two times (at a distance of two days between one and the other) with the same conditioning-amplitude level. The results, shown in Fig. 3, indicate that the time evolution of the modulus and attenuation coefficient are both well reproduced when the experiment is repeated. A similar degree of repeatability is also observed for sample B06.

B. Results

The general behavior of the velocity and attenuation coefficient during conditioning and relaxation is common to the different materials, as shown in Fig. 4. Here, the variations of the velocity and attenuation with respect to their linear values (that is, measured on the relaxed sample and with a low-amplitude excitation) are shown as a function of time for the different samples investigated. In all cases, we observe a common qualitative behavior (in agreement with what is discussed in the theoretical framework reported in Appendix A2).

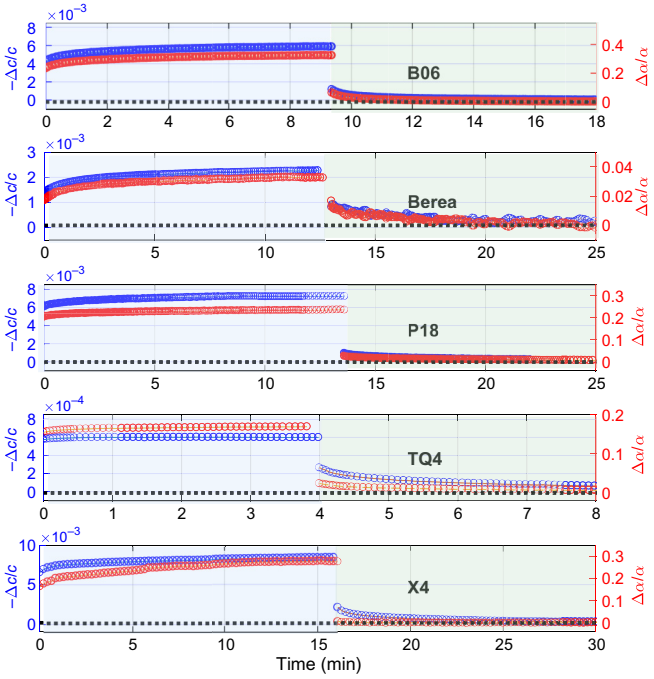

FIG. 4. Relative variation of velocity (blue) and attenuation coefficient (red) during conditioning (left-hand side) and relaxation (right-hand side) for different materials. Note that the sign of the relative variation is inverted for the velocity, to help comparison with the attenuation coefficient.

The results can be summarized as follows:

(a) All the materials feature (i) a softening and an increase in the attenuation coefficient during conditioning, and (ii) a complete relaxation to the original state during relaxation (with hardening and damping reduction).

(b) The time scale for the evolution of conditioning and relaxation is very similar for B06, the Berea Sandstone sample, and P18, that is, those samples with a more homogeneous microstructure. This holds for both the velocity (blue symbols) and the attenuation coefficient (red symbols).

(c) The time scales of conditioning and relaxation for the damaged samples are different.

(d) In the case of B06, the Berea Sandstone sample, and P18, the velocity and attenuation evolve following a qualitatively similar function during both conditioning (left-hand side of the plots) and relaxation (right-hand side). This symmetrical behavior is not featured, however, by samples TQ4 and X4.

(e) Sample TQ4 shows a very small conditioning effect in the velocity (blue symbols), which evolves on a much shorter time scale than the attenuation. The opposite behavior is observed during relaxation, where the damping evolves faster than the velocity. Note that TQ4 shows the highest heterogeneity on the microscale among the samples considered.

(f) In the case of the damaged sample X4, the behavior during conditioning is very similar to that of B06, but, during relaxation, the attenuation coefficient recovers to the preconditioning value much more rapidly, similarly to what is observed for TQ4.

The results reported in Fig. 4 indicate the presence of a number of common features in the processes investigated, but also significant differences, which could be linked to different degrees of heterogeneity at the microstructural level; this is higher for TQ4 and X4 (at least in the area close to the damage location). This suggestion has to be investigated further and more deeply, and might be useful for modeling. Also, differences in the slow-dynamics response of a material to an external excitation could pave the way for novel techniques for materials characterization and damage detection. We will not discuss these issues further, as they need an extensive analysis, together with imaging of the real sample structure, in order to obtain a quantitative description.

Figure 5 shows how the variation in the conditioning amplitude affects the slow dynamics. In all cases (here, only data for B06 are shown), nonequilibrium effects become stronger with increasing amplitude and, at least in the range of excitation levels considered here, no saturation of the effects seems to occur.

Figure 6 reports the results obtained for different conditioning protocols, in panels (a)–(c). First (red curves), an intermediate conditioning amplitude ($A_{inp} = 0.58$ V) is applied to the sample, which is then allowed to relax.

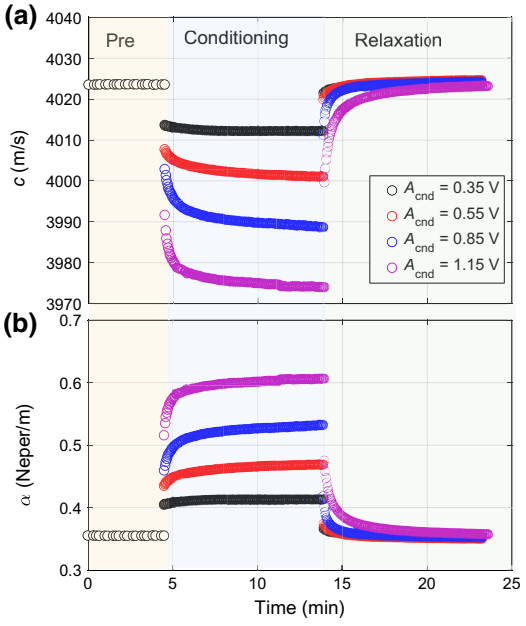

FIG. 5. Evolution of velocity and attenuation coefficient during conditioning and relaxation for different values of the conditioning amplitude for sample B06.

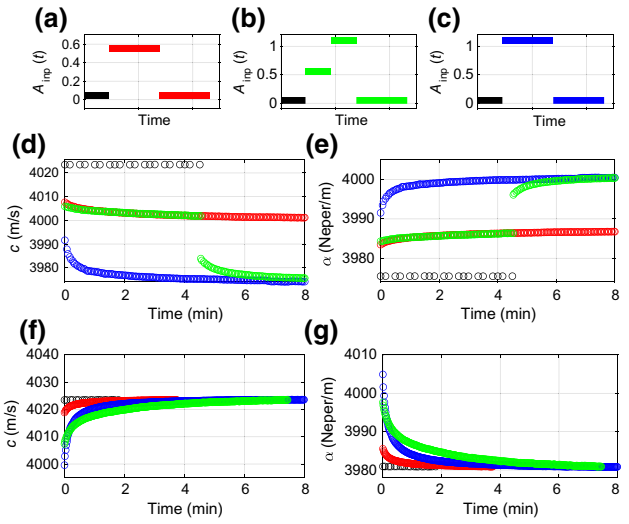

FIG. 6. Evolution of velocity and attenuation coefficient for sample B06 during conditioning for different experimental protocols. (a)–(c) Experimental protocols. Black symbols refer to preconditioning measurements, red symbols to conditioning at $A_{\mathrm{cnd}} = 0.58$ V, blue symbols to conditioning at $A_{\mathrm{cnd}} = 1.2$ V, and green symbols to conditioning at successively increasing conditioning amplitudes. (d) and (e) Conditioning measurements. (f) and (g) Relaxation measurements.

Second (green), the intermediate conditioning amplitude is followed by a larger amplitude ($A_{\mathrm{inp}} = 1.2$ V) and then relaxation is recorded. Third (blue), the large conditioning amplitude is applied directly without any intermediate conditioning step. The results for the evolution of the velocity and attenuation coefficient during conditioning are reported in the respective colors in panels (d) and (e), while their evolution during relaxation is shown in panels (f) and (g). Black symbols refer to results obtained during preconditioning. We can notice the excellent reproducibility of the conditioning step at the intermediate amplitude [superposition of green and red lines in panels (d) and (e)]. Moreover, the behavior of the relaxation process following the application of the large conditioning amplitude is also quite repeatable [superposition of blue and green curves in panels (f) and (g)]. Despite some differences, we consider this result excellent, taking into account the different durations of conditioning at $A_{\mathrm{inp}} = 1.2$ V in the two cases, which is about twice as long in the case of the blue curve. The experimental results shown here agree well qualitatively with the theoretical predictions reported in Fig. 12(b).

IV. DISCUSSION

A. Correlation between velocity and attenuation coefficient

It is interesting, from a theoretical point of view, to quantitatively analyze the existence of correlations between

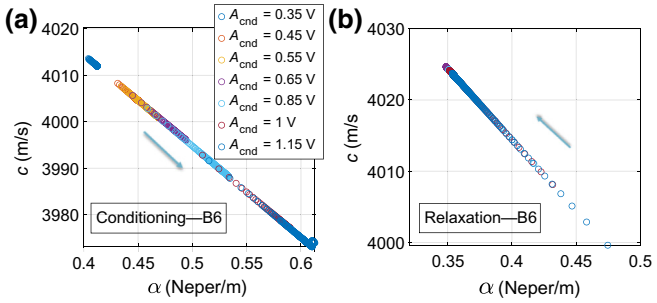

FIG. 7. Parametric plot of c vs α for sample B06 during conditioning and relaxation at different conditioning amplitudes.

the evolution of the attenuation coefficient and that of the velocity during both conditioning and relaxation. Indeed, the presence of such a correlation implies that, most probably, the same physical features (for example, grain contacts or fluids at grain-grain interfaces) are responsible for the observed nonequilibrium effects for both of these physical properties of the material.

Figure 7 shows a plot of c vs α for conditioning (a) and relaxation (b) for sample B06. The value of the velocity at a given time is reported as a function of the attenuation coefficient value obtained at the same time. Different colors refer to different conditioning amplitudes. An excellent linear correlation is observed:

$$c = m\alpha. \tag{1}$$

As mentioned, the existence of a linear correlation between the attenuation coefficient and velocity indicates that the variations in the velocity and damping are proportional to some density N related to microscopic features:

$$\delta_c = k_c N,$$
$$\delta_\alpha = k_\alpha N.$$

We thus have $m = k_c/k_\alpha$, which, in the case of B06, is independent of the conditioning amplitude. From the physical point of view, this fact implies that, at each amplitude, the nonlinear features responsible for hysteresis and nonequilibrium behavior influence the changes in the velocity and attenuation coefficient in the same way.

A linear correlation is also found for other materials, as shown in Fig. 8. In all cases, a linear correlation at a given amplitude of conditioning is found, for both conditioning and relaxation. The correlation coefficient m [see Eq. (1)] is almost independent of the conditioning amplitude in the case of sample P18 also (and should be so for most materials). However, this is not the case for the damaged sample X4, thus denoting an additional difference in the behavior besides that already noticed in Fig. 4.

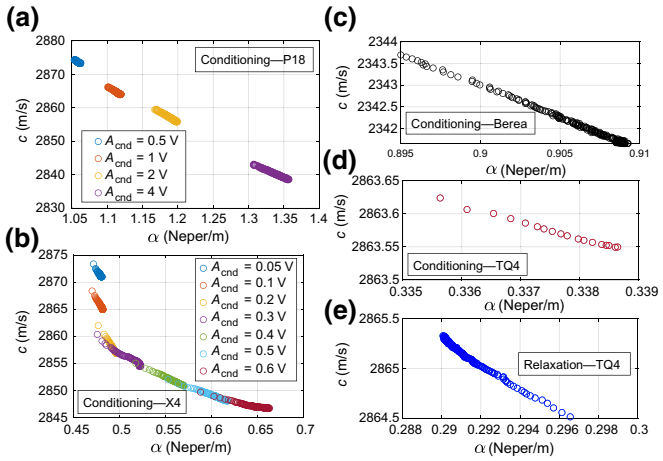

FIG. 8. Parametric plot of c vs α for different samples during conditioning and relaxation.

B. Correlation between conditioning and relaxation

It is also interesting to examine whether the physical elements which undergo conditioning are the same as those responsible for relaxation. In order to shed light on this point, we need to investigate the possible correlations between the parameters describing the behavior of the conditioning and relaxation processes. As shown in Fig. 2 and discussed in Appendix A2, we identify three parameters for the velocity, δc_{NL}, δc_{neq}, and δc_{rlx}, and three for the attenuation coefficient, $\delta\alpha_{\mathrm{NL}}$, $\delta\alpha_{\mathrm{neq}}$, and $\delta\alpha_{\mathrm{rlx}}$.

The dependence of the three parameters on the conditioning amplitude is analyzed in Fig. 9 for the case of sample B06. A linear dependence is found, but with a slightly higher slope (i.e., stronger contribution) for the parameters δc_{NL} and $\delta\alpha_{\mathrm{NL}}$, related to purely nonlinear effects, than for the parameters related to nonequilibrium effects. More important, however, is the fact that the fitting lines, shown as dashed lines in the two panels of Fig. 9, go through the origin only for the nonlinearity parameters. Thus, while purely nonlinear effects do not show an amplitude threshold for their appearance, this does not seem to

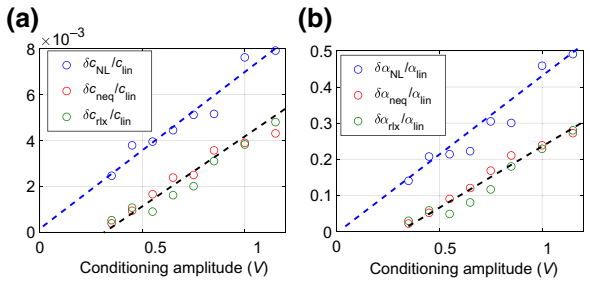

FIG. 9. Evolution of the nonlinear (blue), conditioning (red), and relaxation (green) parameters [see Eqs. (A6) and (A7) and Fig. 2] as a function of conditioning amplitude for sample B06. The dashed lines show linear fits of the data.

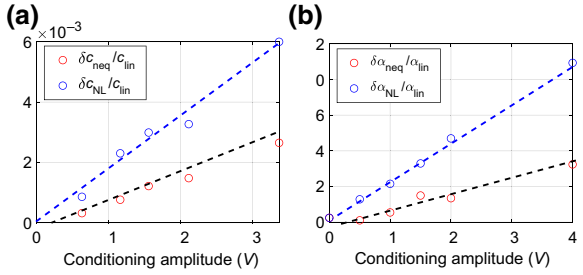

FIG. 10. Evolution of the nonlinear (blue symbols) and conditioning (red symbols) parameters [see Eqs. (A6) and (A7) and Fig. 2] as a function of conditioning amplitude for sample P18. The dashed lines show linear fits of the data.

be the case for nonequilibrium effects. TenCate *et al.* [24] had already postulated the existence of a threshold for the emergence of hysteresis in Berea Sandstone, even though their data did not allow one to decide whether nonequilibrium effects at low excitation amplitudes were absent or were simply hidden below the noise level.

In Fig. 9 it should also be noticed that, in the case of sample B06, $\delta c_{\mathrm{neq}} \approx \delta c_{\mathrm{rlx}}$ and $\delta\alpha_{\mathrm{neq}} \approx \delta\alpha_{\mathrm{rlx}}$, thus supporting the idea that a specific physical signature changes state during conditioning, influencing at the same time the velocity and the attenuation coefficient, and the very same feature relaxes back during the recovery process.

The same dependencies of the slow-dynamics parameters on the conditioning amplitude are observed for sample P18 as well, as shown in Fig. 10, for which conditioning is monitored as a function of amplitude (relaxation is not studied in these experiments). We also note here that in the case of the damaged sample X4 we do not find a clearly defined dependence of the three parameters on the amplitude. Indeed, their distribution is rather scattered. The results are not shown here and could be linked either to the strong localized heterogeneity of the sample or to the fact that relaxation to the original state is not always perfectly complete. Therefore, small variations in the original state of the material from one experiment (i.e., at one conditioning amplitude) to another could be present.

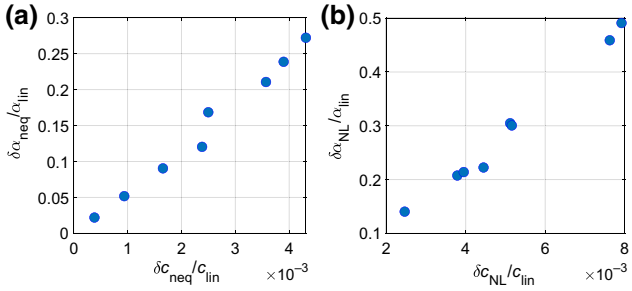

FIG. 11. Attenuation coefficient vs velocity parameter for nonequilibrium (a) and nonlinear (b) effects in sample B06.

The results of our observations regarding the correlation between the attenuation coefficient and the velocity during conditioning are reported in Fig. 11 and are discussed in the Conclusions.

V. CONCLUSIONS

We investigate, experimentally and quantitatively, the effects of conditioning and relaxation in different hysteretic elastic materials as a function of the conditioning amplitude, that is, of the energy of the perturbing waves. The excitations cause fully reversible modifications of the main elastic properties of the samples: the velocity and the attenuation coefficient. Even though conditioning and relaxation have been known in the literature for two decades, we have, to a certain extent, quantified the effect and described some important features of the two phenomena:

(a) For all materials investigated, there is a linear correlation between the evolution of the attenuation coefficient and that of the velocity during slow dynamics, in both the conditioning and the relaxation phases. This implies that the same physical features are causing nonequilibrium effects affecting the modulus and damping, as shown in Fig. 11(a). However, some differences are also evident in the correlation, particularly for the cracked specimen, in which the correlation coefficient seems to be amplitude-dependent or, in other words, the correlation is not linear (Fig. 8). Our results are not conclusive, but indicate that it is highly desirable to further analyze the differences in the behavior of materials with different heterogeneity at the microstructural level and/or with very localized nonlinearity. Moreover, the correlations of the nonequilibrium parameters shown in Fig. 11(a) feature the same qualitative behavior as that of the nonlinear parameters, already well known, reported for the same sample in Fig. 11(b).

(b) For most of the materials analyzed here, correlations exist also between the parameters related to conditioning and relaxation (Fig. 9), thus indicating that the same physical features which are modified during conditioning subsequently relax slowly to their initial physical state. This behavior, however, does not seem to be completely true for the damaged sample, which features nonlinearity and heterogenity at the microscale which is also, most probably, very localized.

The phenomena reported here are very well reproducible (see, for example, Fig. 3), and hence the conclusions drawn are relevant for a deeper comprehension of nonlinear elasticity in mesoscopic elastic materials. Indeed, introducing measurable quantities to characterize slow dynamics and demonstrating that different classes of materials (e.g., intact vs damaged samples) have significantly different behavior (and not only in terms of the strength of the effects) is the first step needed in order to foster applications for materials characterization. Furthermore, since slow dynamics is a peculiar feature of nonclassical nonlinearity, separating effects due to modulus and damping nonlinearity and quantifying them is crucial for understanding the physics behind the phenomenon and linking macroscopic (measurable) ultrasonic observations to microscopic materials features. Further studies will be carried out to extract conclusions with general validity and then to use them both as an input in the determination of the specific physical mechanisms responsible for hysteresis and in applications such as, for example, quantitative nondestructive testing and evaluation.

APPENDIX

1. Determination of velocity and attenuation coefficient

The data analysis used to quantitatively characterize conditioning and relaxation is based on extracting, for each amplitude of excitation, an effective wave velocity c and attenuation coefficient α for the sample considered. This is possible if the propagation medium is quasi-1D, as discussed here. Let us consider the propagation of a monochromatic wave of angular frequency ω in a linear medium of length L. The wave is generated by a forcing transducer located at one end of the specimen ($x = 0$), inducing a longitudinal displacement $A_{\text{inp}}\cos(\omega t + \phi_0)$, which is superimposed on the displacement due to the (multiply reflected) traveling wave. The displacement u recorded at $x = L$ is still a sinusoidal wave, of amplitude B and phase Φ, and an analytical expression for it can be derived by considering the superposition of the multiply reflected waves, as demonstrated in Ref. [47]:

$$u(L,t) = Be^{j(\omega t+\Phi)}, \tag{A1}$$

where

$$B = \frac{A_{\text{inp}}}{\sqrt{\cosh^2(\alpha L) - \cos^2(kL)}}, \tag{A2}$$

$$\Phi = \phi_0 + \phi = \phi_0 - \arctan\left(\frac{\tan(kL)}{\tanh(\alpha L)}\right). \tag{A3}$$

Here, k is the wave number and α the attenuation coefficient.

Equations (A2) and (A3) can be used to extract k and α from experimental data. The amplitude B and phase $\Phi = \phi + \phi_0$ of the signal can be derived by fitting the experimental data with a cosine function, while A_{inp} and ϕ_0 can be obtained through a suitable calibration of the experiment [47]. By inverting Eqs. (A2) and (A3), we obtain the

physical parameters. In particular, we have

$$c = \frac{\omega}{k} = \frac{\omega}{(1/L)\left(\pi n \pm \arctan\sqrt{z/(2\cos^2(\phi))}\right)}, \quad \text{(A4)}$$

$$\alpha = \frac{1}{L}\,\text{arctanh}\sqrt{\frac{z}{2\sin^2(\phi)}}, \quad \text{(A5)}$$

where the sign is plus if $\phi + \phi_0 > 0$, n is the order of the closest mode to ω, and

$$z = -(B/A_{\text{inp}})^2 - \cos(2\phi) + \sqrt{1 + (B/A_{\text{inp}})^4 + 2\cos(2\phi)(B/A_{\text{inp}})^2}.$$

As mentioned before, the solution, which is exact for a linear medium, allows one to obtain the velocity and the attenuation coefficient. For small nonlinear effects, the fitting with a cosine function is still excellent, and Eqs. (A4) and (A5) allow one, for each amplitude (or time, in our case), to extract an "equivalent" attenuation coefficient and velocity.

2. Theory

The results shown in Fig. 2(c) suggest that the behavior of the velocity as a function of strain amplitude should depend on two contributions: the first one, instantaneous, is due to the actual strain, while the second, which is explicitly time-dependent, is related to the maximum amplitude of the strain.

Let us consider a case in which we start with a fully relaxed sample. For each value of the strain, fast dynamics contributes to the velocity with a term δc_{NL}, while conditioning is responsible for a nonequilibrium contribution to the velocity equal to δc_{neq}. Let us assume, for simplicity, that these two terms are independent, and let us define c_L as the linear velocity, that is, the velocity measured at a low excitation amplitude. Then, during conditioning at a given excitation amplitude A_i, the velocity c_i evolves with time as

$$c_i = c_L - \delta c_{i,\text{NL}} - \delta c_{i,\text{neq}} f\,(t - t_c), \quad \text{(A6)}$$

where t_c is the instant at which conditioning starts, and $f(t - t_c)$ is a monotonically increasing function satisfying the condition $f(0) = 0$ and $\lim_{t\to\infty} f(t - t_c) = 1$. Experiments indicate that $f(t - t_c)$ should be approximately a logarithmic function (except at early and asymptotic times), but its exact functional dependence is not relevant in this context. This behavior is qualitatively illustrated in Fig. 12(a).

As soon as the excitation is removed, and the measurements are performed again at a very low excitation amplitude, both the velocity and the attenuation coefficient slowly relax back to the linear value:

$$c_0 = c_L - \delta c_{i,\text{neq}}\,[1 - g\,(t - t_r)], \quad \text{(A7)}$$

where t_r is the instant at which relaxation starts, and $g(t - t_r)$ is again a monotonically increasing function satisfying the condition $g(0) = 0$ and $\lim_{t\to\infty} g(t - t_r) = 1$. The functions $f(t - t_c)$ and $g(t - t_r)$ could, in principle, be different. However, experiments suggest the same functional dependence for both conditioning and relaxation [47].

The situation is more complex when the sample is initially not completely relaxed, that is, when the excitation amplitude is switched from one amplitude A_0 to a larger one A_1 and then is increased again to an even larger value, A_2. This situation is represented, for the conditioning phase, in Fig. 12(b) (red curve). As expected, the final equilibrium value reached is the same as when

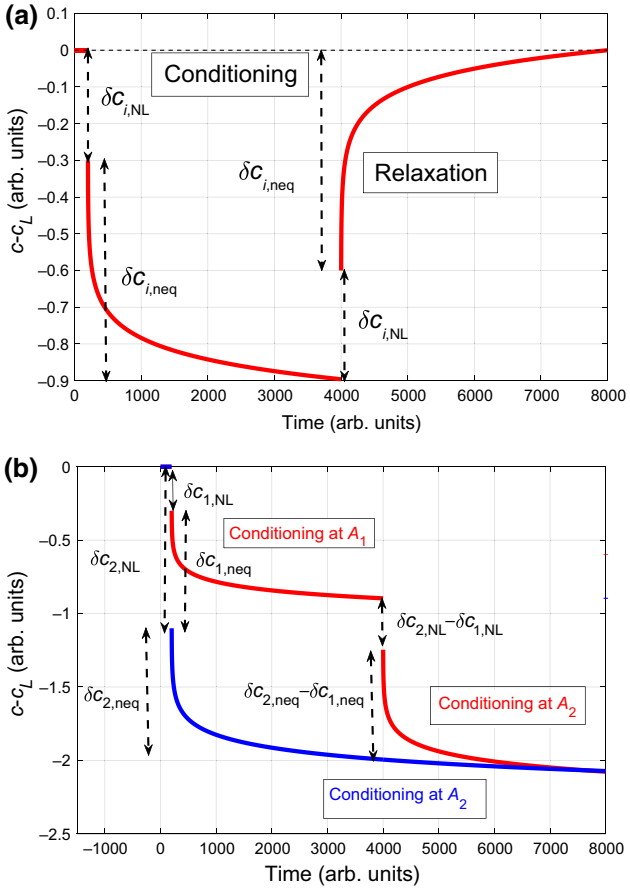

FIG. 12. Upper plot: predictions of the temporal evolution of velocity when the excitation amplitude is switched on (conditioning) and off (relaxation). Lower plot: predictions of the temporal evolution of velocity when the excitation amplitude is switched from A_0 to $A_1 > A_0$ and then to $A_2 > A_1$ (red curve), compared with the case in which the amplitude goes to A_2 directly from A_0 (blue curve).

switching directly from the relaxed state to amplitude A_2 (blue curve). The equation describing the evolution of the velocity during conditioning at amplitude A_2 becomes

$$c_2 = c_1 - \psi - \Phi f(t - t_c), \tag{A8}$$

where t_c is the instant at which the excitation amplitude is switched to the value A_2, $\psi = \delta c_{2,\mathrm{NL}} - \delta c_{1,\mathrm{NL}}$, and $\Phi = \delta c_{2,\mathrm{neq}} - \delta c_{1,\mathrm{neq}}$. Similar considerations hold also for describing relaxation when the excitation amplitude switches back to A_1 and then to A_0.

[1] L. D. Landau and E. M. Lifshitz, *Theory of Elasticity* (Pergamon Press, Oxford, 1986).

[2] R. A. Guyer and P. A. Johnson, *Nonlinear Mesoscopic Elasticity* (Wiley-VCH, Weinheim, 2009).

[3] R. A. Guyer and P. A. Johnson, Nonlinear mesoscopic elasticity: Evidence for a new class of materials, Phys. Today **52**, 30 (1999).

[4] A. A. Shah and Y. Ribakov, Non-destructive evaluation of concrete in damaged and undamaged states, Mater. Des. **30**, 3504 (2009).

[5] P. Antonaci, C. L. E. Bruno, P. G. Bocca, M. Scalerandi, and A. S. Gliozzi, Nonlinear ultrasonic evaluation of load effects on discontinuities in concrete, Cem. Concr. Res. **40**, 340 (2010).

[6] R. A. Guyer, J. TenCate, and P. A. Johnson, Hysteresis and the Dynamic Elasticity of Consolidated Granular Materials, Phys. Rev. Lett. **82**, 3280 (1999).

[7] J. Rivière, P. Shokouhi, R. A. Guyer, and P. A. Johnson, A set of measures for the systematic classification of the nonlinear elastic behavior of disparate rocks, J. Geophys. Res.-Solid Hearth **120**, 1587 (2015).

[8] V. Y. Zaitsev, V. E. Gusev, V. Tournat, and P. Richard, Slow Relaxation and Aging Phenomena at the Nanoscale in Granular Materials, Phys. Rev. Lett. **112**, 108302 (2014).

[9] G. Kim, J.-Y. Kim, K. E. Kurtis, and L. J. Jacobs, Drying shrinkage in concrete assessed by nonlinear ultrasound, Cem. Concr. Res. **92**, 16 (2017).

[10] J. Jin, J. Rivière, Y. Ohara, and P. Shokouhi, Dynamic acousto-elastic response of single fatigue cracks with different microstructural features: An experimental investigation, J. Appl. Phys. **124**, 075303 (2018).

[11] M. Bentahar and R. El Guerjouma, Monitoring progressive damage in polymer-based composite using nonlinear dynamics and acoustic emission, J. Acoust. Soc. Am. **125**, EL39 (2009).

[12] T. J. Ulrich, A. Sutin, T. Claytor, P. Papin, P.-Y. Le Bas, and J. A. TenCate, The time reversed elastic nonlinearity diagnostic applied to evaluation of diffusion bonds, Appl. Phys. Lett. **93**, 151914 (2013).

[13] M. Scalerandi, A. S. Gliozzi, C. L. E. Bruno, and P. Antonaci, Nonequilibrium and hysteresis in solids: Disentangling conditioning from nonlinear elasticity, Phys. Rev. B **81**, 104114 (2010).

[14] M. Li, A. M. Lomonosov, Z. Shen, H. Seo, K.-Y. Jhang, V. E. Gusev, and C. Ni, Monitoring of thermal aging of aluminum alloy via nonlinear propagation of acoustic pulses generated and detected by lasers, Appl. Sci. **9**, 1191 (2019).

[15] I. Solodov, Resonant acoustic nonlinearity of defects for highly-efficient nonlinear NDE, J. Nondestr. Eval. **33**, 252 (2014).

[16] M. Bentahar, H. El Aqra, R. El Guerjouma, M. Griffa, and M. Scalerandi, Hysteretic elasticity in damaged concrete: Quantitative analysis of slow and fast dynamics, Phys. Rev. B **73**, 014116 (2006).

[17] S. Haupert, G. Renaud, J. Rivière, and Maryline Talmant, High-accuracy acoustic detection of nonclassical components of material nonlinearity, J. Acoust. Soc. Am. **130**, 2654 (2011).

[18] A. Carrión, V. Genovés, G. Pérez, J. Payá, and J. Gosálbez, Flipped accumulative non-linear single impact resonance acoustic spectroscopy (FANSIRAS): A novel feature extraction algorithm for global damage assessment, J. Sound Vib. **432**, 454 (2018).

[19] M. Scalerandi, A. S. Gliozzi, C. L. E. Bruno, D. Masera, and P. Bocca, A scaling method to enhance detection of a nonlinear elastic response, Appl. Phys. Lett. **92**, 101912 (2008).

[20] M. Scalerandi, M. Bentahar, and C. Mechri, Conditioning and elastic nonlinearity in concrete: Separation of damping and phase contributions, Constr. Build. Mater. **161**, 208 (2018).

[21] C. Trarieux, S. Callé, H. Moreschi, G. Renaud, and M. Defontaine, Modeling nonlinear viscoelasticity in dynamic acoustoelasticity, Appl. Phys. Lett. **105**, 264103 (2014).

[22] J. A. Ten Cate, E. Smith, and R. A. Guyer, Universal Slow Dynamics in Granular Solids, Phys. Rev. Lett. **85**, 1020 (2000).

[23] R. A. Guyer, K. R. McCall, and K.-E. Van den Abeele, Slow elastic dynamics in a resonant bar of rock, Geophys. Res. Lett. **25**, 1585 (1998).

[24] J. A. TenCate, D. Pasqualini, S. Habib, K. Heitmann, D. Higdon, and P. A. Johnson, Nonlinear and Nonequilibrium Dynamics in Geomaterials, Phys. Rev. Lett. **93**, 065501 (2004).

[25] M. Lott, M. C. Remillieux, V. Garnier, P.-Y. Le Bas, T. J. Ulrich, and C. Payan, Nonlinear elasticity in rocks: A comprehensive three-dimensional description, Phys. Rev. Mater. **1**, 023603 (2017).

[26] J. Rivière, G. Renaud, R. A. Guyer, and P. A. Johnson, Pump and probe waves in dynamic acousto-elasticity: Comprehensive description and comparison with nonlinear elastic theories, J. Appl. Phys. **114**, 054905 (2013).

[27] C. Mechri, M. Scalerandi, and M. Bentahar, Enhancement of harmonics generation in hysteretic elastic media induced by conditioning, Commun. Nonlinear Sci. Numer. Simul. **45**, 117 (2017).

[28] M. Remillieux, R. A. Guyer, C. Payan, and T. J. Ulrich, Decoupling Nonclassical Nonlinear Behavior of Elastic Wave Types, Phys. Rev. Lett. **116**, 115501 (2016).

[29] J. A. Ten Cate and T. J. Shankland, Slow dynamics in the nonlinear elastic response of Berea sandstone, Geophys. Res. Lett. **23**, 3019 (1996).

[30] J. A. Bittner and J. S. Popovics, Direct imaging of moisture effects during slow dynamic nonlinearity, Appl. Phys. Lett. **114**, 021901 (2019).

[31] A. Astorga, P. Guéguen, and T. Kashima, Nonlinear elasticity observed in buildings during a long sequence of earthquakes, Bull. Seism. Soc. Am. **108**, 1185 (2018).

[32] M. Scalerandi, S. Idjimarene, M. Bentahar, and R. El Guerjouma, Evidence of microstructure evolution in solid elastic media based on a power law analysis, Commun. Nonlinear Sci. Numer. Simul. **22**, 334 (2015).

[33] M. Scalerandi, Power laws and elastic nonlinearity in materials with complex microstructure, Phys. Lett. A **380**, 413 (2016).

[34] G. Shkerdin and C. Glorieux, Nonlinear modulation of Lamb modes by clapping delamination, J. Acoust. Soc. Am. **124**, 3397 (2008).

[35] C. Pecorari, Adhesion and nonlinear scattering by rough surfaces in contact: Beyond the phenomenology of the Preisach-Mayergoyz framework, J. Acoust. Soc. Am. **116**, 1938 (2004).

[36] E. Shalev, V. Lyakhovsky, A. Ougier-Simonin, Y. Hamiel, and W. Zhu, Inelastic compaction, dilation and hysteresis of sandstones under hydrostatic conditions, Geophys. J. Int. **197**, 920 (2014).

[37] S. Delrue, V. Aleshin, K. Truyaert, O. Bou Matar, and K. Van Den Abeele, Two dimensional modeling of elastic wave propagation in solids containing cracks with rough surfaces and friction – Part II: Numerical implementation, Ultrasonics **82**, 19 (2018).

[38] H. Berjamin, N. Favrie, B. Lombard, and G. Chiavassa, Nonlinear waves in solids with slow dynamics: An internal-variable model, Proc. Royal Soc. A Math. Phys. Eng. Sci. **473**, 20170024 (2017).

[39] C. K. C. Charles, E. G. Daub, R. E. Ecke, and P. A. Johnson, Slow dynamics and strength recovery in unconsolidated granular earth materials: A mechanistic theory, J. Geophys. Res.-Sol. Earth **122**, 7573 (2017).

[40] M. Nobili and M. Scalerandi, Temperature effects on the elastic properties of hysteretic elastic media: Modelling and simulations, Phys. Rev. B **69**, 04105 (2004).

[41] C. W. MacMinn, E. R. Dufresne, and J. S. Wettlaufer, Large Deformations of a Soft Porous Material, Phys. Rev. Appl. **5**, 044020 (2016).

[42] J. N. Eiras, Q. A. Vu, M. Lott, J. Payá, V. Garnier, and C. Payan, Dynamic acoustoelastic test using continuous wave probes and transient vibration to investigate material nonlinearity, Ultrasonics **69**, 29 (2016).

[43] J. Jin, M. G. Moreno, J. Riviere, and P. Shokouhi, Impact based nonlinear acoustic testing for characterisation of distributed damage in concrete, J. Nondestruct. Eval. **36**, 51 (2017).

[44] P. Gueguen, P. A. Johnson, and P. Roux, Nonlinear dynamics induced in a structure by seismic and environmental loading, J. Acoust. Soc. Am. **140**, 582 (2016).

[45] P. Shokoui, J. Rivière, C. R. Lake, P.-Y. Le Bas, and T. J. Ulrich, Dynamic acousto-elastic testing of concrete with a coda-wave probe: Comparison with standard linear and nonlinear techniques, Ultrasonics **81**, 59 (2017).

[46] Q. A. Vu, V. Garnier, J. F. Chaix, C. Payan, M. Lott, and J. N. Eiras, Concrete cover characterisation using dynamic acoustoelastic testing and Rayleigh waves, Constr. Build. Mater. **114**, 87 (2016).

[47] C. Mechri, M. Scalerandi, and M. Bentahar, Separation of Damping and Velocity Strain Dependencies Using an Ultrasonic Monochromatic Excitation, Phys. Rev. Appl. **11**, 054050 (2019).